ACS APPLIED MATERIALS & INTERFACES

www.acsami.org

Research Article

Spallation of Isolated Aluminum Nanoparticles by Rapid Photothermal Heating

Naadaa Zakiyyan, Cherian Mathai, Jacob McFarland, Shubhra Gangopadhyay,* and Matthew R. Maschmann*

Cite This: *ACS Appl. Mater. Interfaces* 2022, 14, 55277−55284

Read Online

ACCESS | Metrics & More | Article Recommendations | Supporting Information

ABSTRACT: The spallation of isolated aluminum (Al) nanoparticles (NPs) is initiated using rapid photothermal heating. The Al NPs exhibited a nominal diameter of 120 nm, with an average oxide shell thickness of 3.8 nm. Photothermal heating was achieved by coupling a focused laser (446 nm wavelength) to an optical grating substrate and to the plasmonic resonance of the Al NPs themselves. These factors enhanced the absorption cross section by a factor of 8−18 compared to no substrate and generated an Al NP heating rate on the order of 10^7−10^8 K/s. Observations indicate that molten Al is ejected from the heated NP, indicating that melting of the Al core is required for spallation. A graphene layer atop the grating substrate encouraged the formation of discrete particles of ejected Al, while irregular elongated filament products were observed without the graphene layer. Numerical simulations indicate that laser-heated Al NPs reach temperatures between approximately 1000 and 1500 K. These observations and experimental conditions are consistent with those anticipated for the melt dispersion mechanism, a thermomechanical reaction mechanism that has not previously been clearly demonstrated. Activating and controlling this mechanism is anticipated to enhance applications ranging from biological phototherapy to energetic materials.

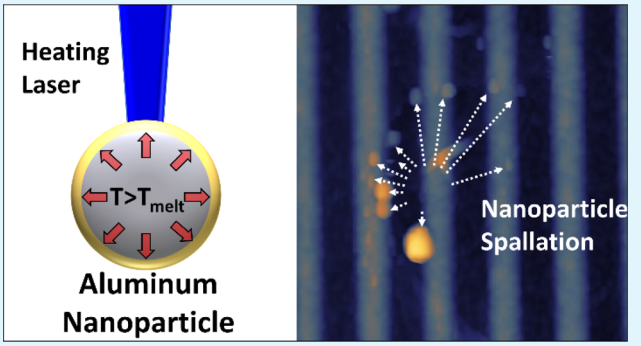

KEYWORDS: *aluminum, nanoparticles, plasmonic grating, photothermal, spallation*

1. INTRODUCTION

Aluminum (Al) nanoparticles (NPs) are energetic materials that have attracted interest because of their high energy density, low cost, and commercial availability.[1−3] Applications of Al NPs include solid propellants, explosives, hydrocarbon fuel additives, and enhanced combustion of metastable intermixed composites.[4−7] To react with surrounding oxide, the metallic Al core must escape an encapsulating alumina shell. Understanding and controlling the fundamental escape mechanisms of Al fuel through the shell is crucial to optimizing their use in diverse applications. Various mechanisms have been proposed based upon the NP heating rate, including the diffusion oxidation mechanism (DOM) and melt dispersion mechanism (MDM).[8−16] The DOM is observed in a slower heating rate regime (10^4−10^6 K/s), in which the reaction is initiated by diffusion of the Al and O atoms through the core−shell interface or the outer surface of the Al NP.[17] In the DOM, Al diffusion through the amorphous Al_2O_3 shell restricts the reaction rate between the metallic fuel and surrounding oxide. The outward diffusion of Al is more rapid than the inward diffusion of oxygen (O), causing coarsening of the amorphous oxide layer, as shown by molecular dynamics simulation and experimental observations.[18,19] At a temperature of 770 K, a polymorphic phase transformation of the oxide shell may initiate the nucleation of high-density crystallites.[20] These crystallites are accompanied by the formation of small voids at their boundaries that may accelerate the escape of Al.[21,22] The thermomechanical MDM model proposes that rapid heating, melting, and expansion of the Al core produce sufficiently high hoop stress on the alumina shell to induce mechanical failure and spallation of the Al core. Activation of this effect requires specific conditions, including very high heating rates (10^6−10^9 K/s), a core temperature that exceeds the melting temperature of Al (934 K), and a sufficiently homogeneous alumina shell that can withstand the building pressure provided by the Al core.[23] Shells with preexisting defects, including nanovoids, impurities, and heterogeneous shell thickness, may hinder the occurrence of MDM.[24,25]

Promoting the rapid spallation and ejection of molten Al fuel, as proposed by the MDM model, could drastically

Received: October 17, 2022
Accepted: November 10, 2022
Published: November 29, 2022

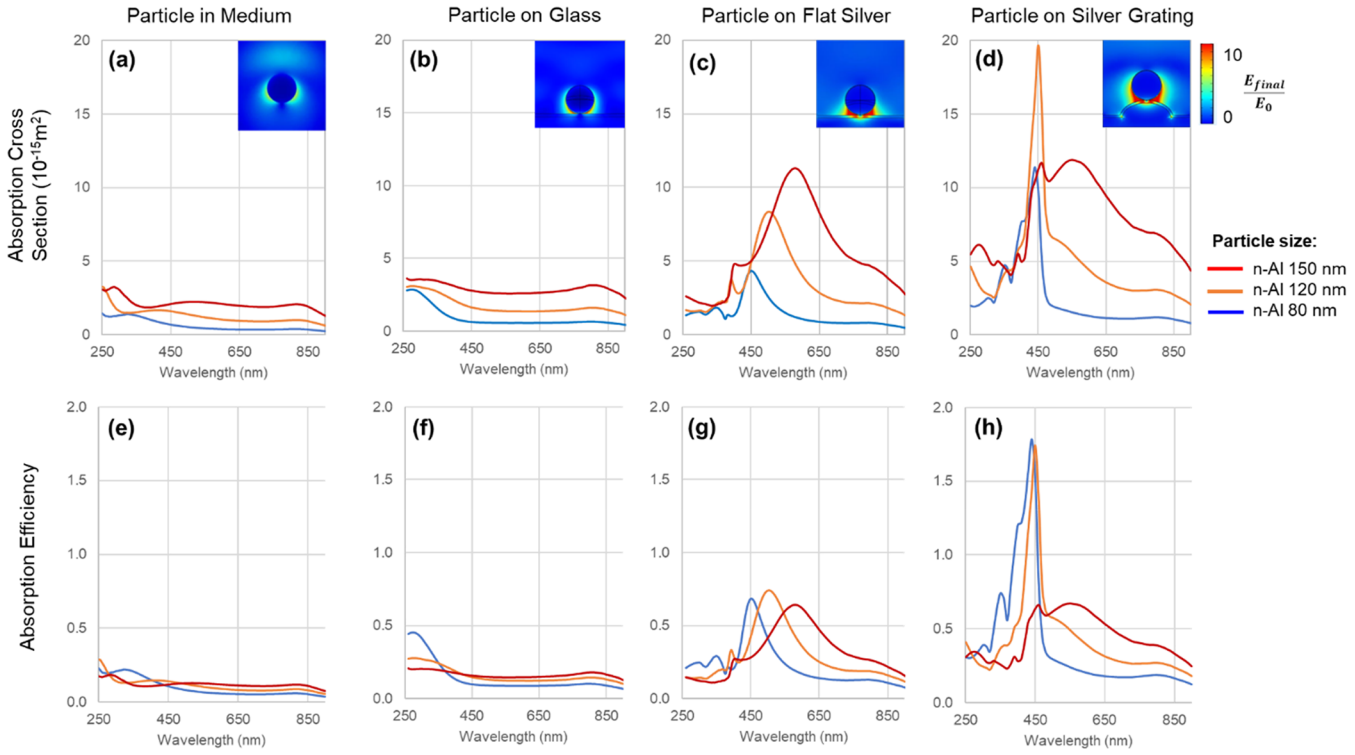

Figure 1. Al NP spectral absorption simulated using *COMSOL Multiphysics 5.2a*: (a–d) absorption cross section; (e–h) absorption efficiency in an air medium for a single Al NP suspended in a medium, on a glass substrate, on a glass substrate with a reflective Ag film, and on a Ag-coated grating, respectively.

increase the reaction rates of nanothermite systems. However, experimental validation of MDM, or other dispersive reaction mechanisms, has not been clearly presented in the literature. Several different heating schemes have been attempted to observe MDM. One such experiment used photothermal heating of nanoscale Al disks fabricated using electron-beam lithography and Al evaporation.[26] The disks were patterned with a diameter of 400 nm and a pitch of 500 nm to activate plasmonic coupling with a 532-nm-wavelength laser. The experiment achieved a heating rate of 0.88×10^6 K/s based on the reported maximum temperature and laser pulse times, approaching the threshold heating of 10^6 K/s to initiate MDM. The maximum temperature of the Al disks was 975 K, just above the Al melting temperature. While the MDM was proposed for this experiment, no ejected particles were observed, even in scanning and transmission electron microscopy (SEM and TEM) images. In situ infrared imaging also failed to detect flame generation. In another attempt to isolate the MDM, clusters of approximately 100 Al NPs were heated using a 12-ns-pulsed 1064-nm-wavelength laser or a thin-film micro/electromechanical system (MEMS) heater within a transmission electron microscope.[27] The Al NPs were nominally 80 nm in diameter, with an estimated 3 nm oxide shell thickness. These TEM experiments failed to demonstrate Al spallation, but adjacent NPs coalesced to form a large particle without evidence of the MDM. The estimated heating rates of the Al NPs ranged between 10^6 and 10^{11} K/s; however, the potential underestimation of the alumina shell thickness and insufficient temperature to induce the MDM may explain the observed sintering mechanism rather than the MDM.[25] A similar experiment using a thin-film MEMS-based heater that generated a 10^6 K/s heating rate failed to produce Al NP spallation even in the presence of WO_3 oxide NPs.[28] A clear set of experiments that examine isolated Al NPs without an oxidizer and clearly meet and exceed the MDM threshold heating parameters are needed to conclusively validate the proposed spallation mechanism.

2. MATERIALS AND METHODS

The electric-field distribution and transient thermal response were simulated numerically using finite-element software (*COMSOL Multiphysics 5.2a*). The numerical simulations have been used in numerous recent reports[33−35] and were preferable to the analytical solution in solving partial differential equations (PDEs) for heterostructured models. The baseline spectral absorption of an Al NP surrounded by air was first evaluated and represented by the absorption cross section based on the Mie theory (Figure 1). An individual NP of 90, 120, or 150 nm diameter was simulated with a 3 nm alumina shell. The same Al NP was then simulated while resting on the ridge of a plasmonic grating substrate to determine the electric-field enhancement. A horizontal span of three grating pitches was modeled to reduce the computational workload, while the scattering boundary condition was applied so that no inward waves were entering the domain. A transverse magnetic (TM)-polarized electric-field source was placed 1.2 μm above the grating at 0° incident angle, normal to the substrate. TM polarization is desired for coupling, while the electric component of the incident electromagnetic wave is parallel to the plane of incidence. The electric-field source is represented as a uniform intensity with a peak power density of 4.2×10^5 W/cm^2. The transient thermal response of Al NPs on the grating surface was then modeled by using the Al NP energy absorption as an input to the 3D heat equation solved using *COMSOL Multiphysics 5.2a*. In the heat-transfer simulation, a larger model dimension of $10 \times 10 \times 1.2$ μm^3 was applied, with the Al NPs acting as the heat source. Most particles contacted the underlying grating, which itself served as a heat sink. Melting and solidification of a Al NP was explicitly considered to be the product of the Al NP mass and the latent heat of fusion (396 J/g). The bulk Al melting temperature was used because previous studies demonstrated that the dimension[36] and

https://doi.org/10.1021/acsami.2c18678
ACS Appl. Mater. Interfaces 2022, 14, 55277−55284

alumina shell[37] negligibly suppress the melting temperature of 120-nm-diameter particles.

Optical microscopy was used to identify and photothermally heat isolated clusters of Al NPs. The Al NPs had a nominal diameter of 120 nm (Novacentrix M2692 Al-120-P). TEM analysis showed an average NP diameter of 111 ± 26 nm with an oxide thickness of 3.8 ± 1.0 nm. The Al NPs were dispersed in isopropyl alcohol (0.01 mg/mL) and sonicated for 2 h before their dispersal on the grating substrate. Then, 5 μL of the Al NPs solution was drop-casted onto the sample and air-dried before heating experiments were performed.

A plasmonic grating microchip was fabricated using a microcontact lithography stamping process.[29] HDDVD gratings were negatively copied using poly(dimethylsiloxane) stamping and then replicated in poly(methylsilsesquioxane) with an added cross-linker, 3-(aminopropyl)triethoxysilane. The HDDVD substrate produced a grooved substrate with a 400 nm pitch and a 60 nm peak-to-valley ridge height.[30,31] A 100-nm-thick film of silver (Ag) and a 10-nm-thick protective layer of alumina (Al_2O_3) were deposited on the grating by sputtering and atomic layer deposition (ALD), respectively. To differentiate between the Ag grains on the grating and the postreaction products when using atomic force microscopy (AFM) imaging, a single-layer graphene sheet (Trivial Transfer Graphene, ACS Material) was placed on the grating substrate.[32] The presence of a graphene layer was verified by Raman spectroscopy and SEM.

Diode lasers with wavelengths of 446, 638, and 808 nm were used as photothermal heating sources. All lasers were introduced by the optical path of a microscope (Olympus BX51) and focused through the microscope objective. The 446-nm-wavelength laser used a 100× air objective, while the 638 and 808 nm lasers used a 100× oil objective to improve coupling. These laser-wavelength sample spectra corresponded to high (446 nm), moderate (638 nm), and low (808 nm) absorption efficiencies provided by the grating substrate. The 446 nm laser profile has dimensions of 1.1 μm × 0.4 μm and can be observed by the dashed outline in Figure 2. The profile represents the full-width half-maximum (fwhm) of the laser profile. The 446 nm laser had a 7 μs rise time to reach a peak power of 7.6 mW and a power density of 4.2 × 10^5 W/cm^2 (Figure S1). The 635- and 808-nm-wavelength lasers utilized a 125 μs rise time, with peak power densities of 7.7 × 10^5 and 8.6 × 10^5 W/cm^2, respectively. The longer rise times were required to ensure that Al NPs reached their melting temperature.

A Bruker Innova atomic force microscope was used in tapping mode to quantify sample topology before and after selected laser heating experiments. A 2 nm radius probe tip (NanoAndMore) was used for scanning. The typical AFM scan area was 3 μm × 3 μm. Line scans proceeded at a rate of 0.5 Hz with a resolution of 1024 × 1024 pixels. Topology analysis was performed using *Gwyddion* software.

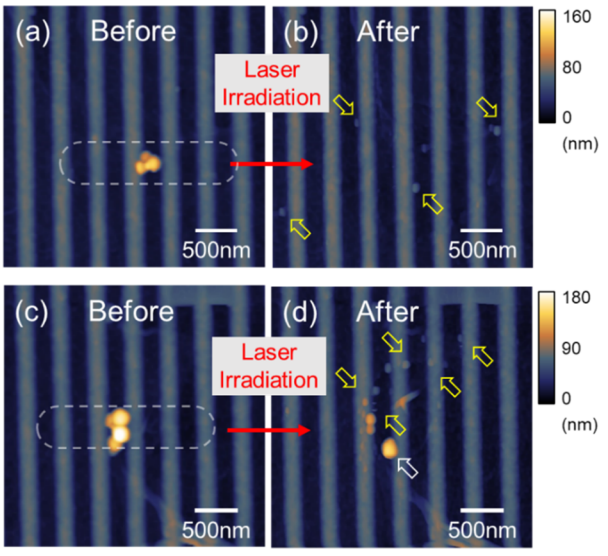

Figure 2. Evolution of Al NP morphology due to laser irradiation as measured by AFM. (a and c) AFM images show Al NPs residing on a plasmonic grating microchip with a graphene overlayer. The dashed line represents the fwhm of the laser spatial profile. (b and d) After a laser pulse irradiated the NPs, AFM images show fragment dispersal locations indicated by yellow arrows and an unreacted particle indicated by the white arrow. The periodic ridges represent the plasmonic grating substrate.

3. RESULTS AND DISCUSSION

Spectral absorption was simulated for an Al NP residing in an air medium, on a glass slide, on flat silver surface, and on the plasmonic grating. The results, in Figure 1, are presented with respect to the absorption cross section and absorption efficiency. The spectral absorption plot (Figure 1) for isolated Al NPs shows that the dielectric loss peak is located at 810 nm for all Al NP diameters, while the plasmonic peaks redshift and broaden as the Al NP diameter increases, similar to other reports.[38] The absorption between 350 and 850 nm wavelength is greatly enhanced by the flat silver and grating substrates. The absorption is most pronounced at 450 nm wavelength on the grating substrate, near its plasmonic resonance. A 120-nm-diameter Al NP on the grating substrate experiences an absorption enhancement of approximately 5 times at 450 nm wavelength compared to a flat silver substrate and approximately 10 times compared to a flat glass substrate. We were unable to differentiate enhancement factors arising from the grating and localized surface plasmon resonance of the NPs themselves.

In laser heating experiments, individual Al NPs exhibited no morphological changes before and after heating, indicating no reaction, as shown in Figure S2. COMSOL simulations confirm that individual Al NPs do not reach their melting temperatures. Clusters comprised of multiple Al NPs in contact were selected for spallation experiments to increase the quantity of heating sources and further enhance the Al NP absorption efficiency.[39] AFM topology images, shown in Figure 2a,c, display representative clusters of Al NPs prior to laser heating experiments. The well-defined grating surface indicates that the graphene sheet conformed well to the grating surface.

Evidence for spallation in response to photothermal heating can be observed within clusters of four Al NPs using AFM topology images, as displayed in Figure 2b. This figure represents the Al NPs shown in Figure 2a after 446 nm laser pulse irradiation. No evidence of the original Al NPs was observed after the heating in Figure 2b; instead, a dispersal pattern of smaller fragments was present that extended radially more than 500 nm beyond the initial perimeter of the original cluster. Considering that laser-induced heating occurred within the 7 μs irradiation time and assuming that Al melting temperature (934 K) was the minimum temperature required to facilitate spallation, a heating rate of approximately 10^8 K/s may be estimated. The dispersed NP fragments suggest a rapid material release generated from high pressure, with no large fragments (>50 nm) discernible after the reaction. All Al NPs in the original cluster received uniform irradiation in this example because all particles were within the area defined by the laser profile, overlaid on Figure 2a.

By contrast, parts c and d of Figure 2 show a cluster of Al NPs in which one NP was located slightly outside the peak laser intensity. The lower-most particle resided outside the central heating zone and experienced a laser flux approximately

https://doi.org/10.1021/acsami.2c18678
ACS Appl. Mater. Interfaces 2022, 14, 55277−55284

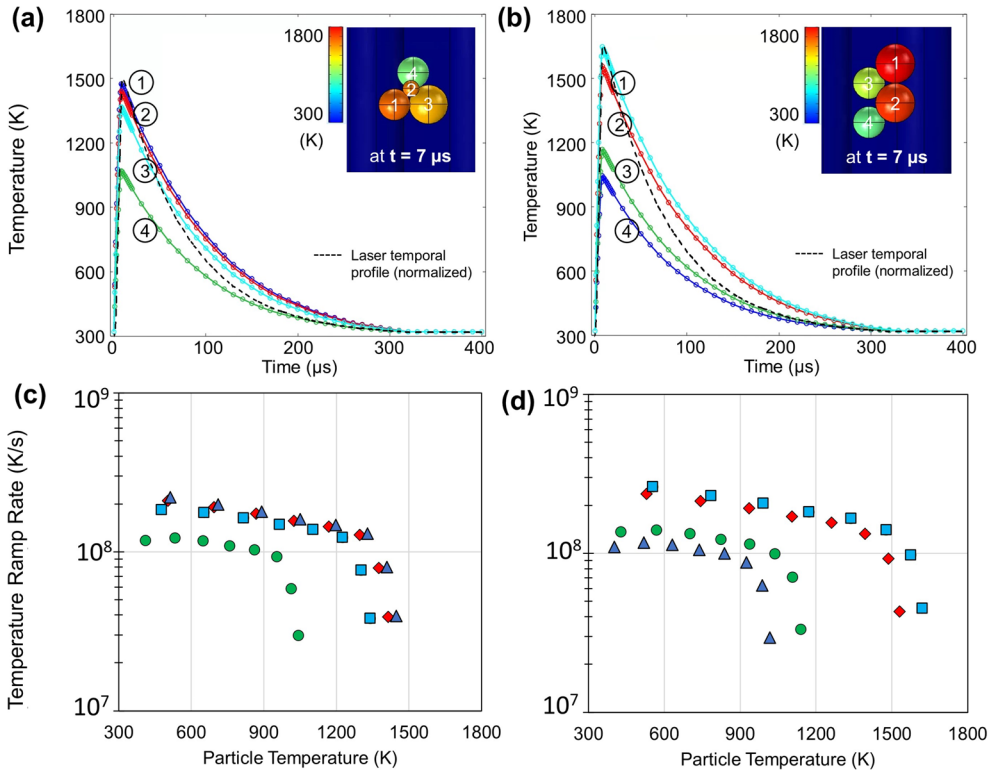

Figure 3. (a and b) Transient thermal responses of Al NPs modeled in COMSOL based on particle arrangements in Figure 2. Particle core temperature of the corresponding four Al NPs (insets). The laser temporal profile is plotted as a black dotted line and normalized to the peak temperature. (c and d) Temperature ramp rate from parts a and b, respectively, plotted as a function of the corresponding particle temperature.

60% lower than that of the surrounding particles. While the three Al NPs that received the full laser irradiation intensity appear to have experienced spallation (yellow arrows), the particle that received lower laser fluence did not rupture, as observed by the lower-most particle in Figure 2d (white arrow). Notice that the graphene wrinkles at the bottom center of Figure 2c,d provide a fiducial reference point. Accordingly, the large particle translated approximately 250 nm to the right during the reaction, from the left side of a grating through the right side. Fragment particles smaller than 50 nm observed on the graphene sheet may represent Al from the core or alumina shell fragments. Energy-dispersive X-ray spectroscopy via SEM was attempted but could not distinguish the composition of the fragmented material because of the small feature size and significant alumina layer contained within the underlying grating structure.

COMSOL was used to simulate Al NP configurations similar to the clusters experimentally observed in Figure 2a,c. The model incorporated the AFM-measured size (based on topology) and morphological arrangement of the Al NPs relative to the grating substrate to match the actual experimental conditions as closely as possible. The simulated transient temperature for each particle within the two cluster configurations is shown in Figure 3. Each particle featured a volumetric energy generation term consistent with the simulated energy absorption, which was consistent with our previous reports.[40] Previous experiments confirmed that the grating itself generates negligible heating during irradiation.[41] A more detailed simulation configuration and results can be seen in Figure S3. The nearly constant temperature ramp rate, shown in the offsets of Figure 3, is a key feature in the transient temperature profiles and results from the 7 μs (446 nm) laser rise time. Note that a ramp rate on the order of 10^7–10^8 K/s is modestly greater than the MDM threshold value of 10^6 K/s. The flux and rise time of the laser produce an energy density of 1.5 J/cm^2. Previous studies indicated that a flux of 5 J/cm^2 is sufficient to induce Al ablation when using nanosecond-pulsed lasers.[42] The energy density and rise time of the laser, coupled with the plasmonic enhancement provided by the grating substrate, are likely key contributors to the spallation observed herein.

Table 1 summarizes the simulated peak temperature for all NPs in Figure 3 corresponding to the experimental configurations of NPs observed in Figure 2. All particles in the simulation reached the Al melting temperature of 934 K. The Al NP that fell outside of the area of maximum laser intensity (denoted in Table 1 as particle 4 in Figure 3b) reached the melting temperature, but insufficient energy was supplied for full melting. This Al NP remained after irradiation experiments (Figure 2c,d), while the other NPs in the cluster experienced spallation, suggesting relative agreement between simulation and modeling.

Table 1. Peak Temperatures for All NPs Simulated in COMSOL

	Figure 3a		Figure 3b	
particle	diameter (nm)	peak temperature (K)	diameter (nm)	peak temperature (K)
1	120	1342	150	1515
2	60	1308	150	1424
3	120	1235	120	1035
4	150	937	120	934

https://doi.org/10.1021/acsami.2c18678
ACS Appl. Mater. Interfaces 2022, 14, 55277−55284

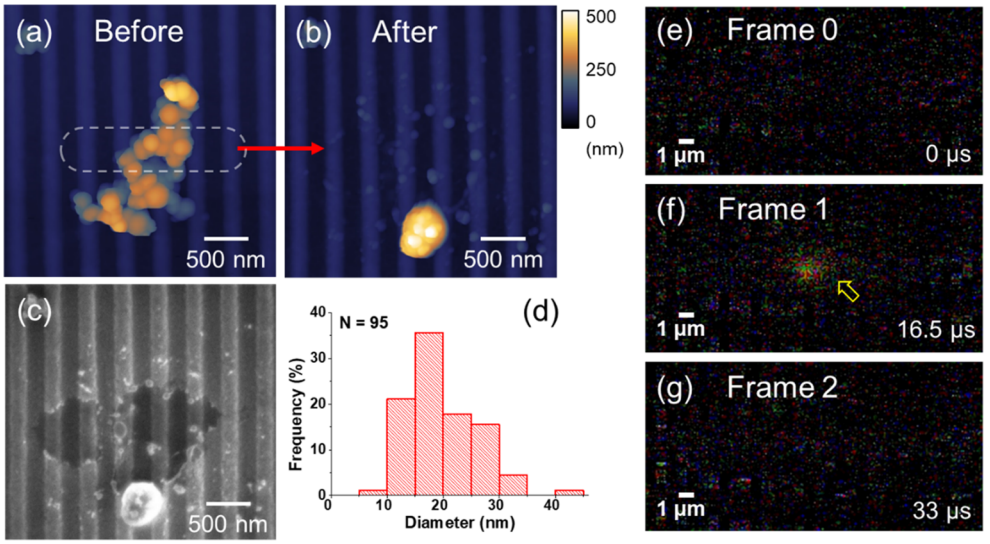

Figure 4. (a) AFM images of Al NPs residing on a plasmonic grating microchip with graphene overlay. High-resolution (b) AFM and (c) SEM images revealing postreaction products after a laser pulse irradiated the NPs. (d) Histogram of the size distribution of the dispersed nanofragments. (e–g) High-speed image capturing light emitted from the spallation reaction.

According to the MDM, spallation is triggered at a temperature that meets or exceeds the Al melting temperature. As the ratio of the shell thickness to the Al radius increases, the spallation threshold temperature increases.[25] In other words, larger-diameter particles are expected to be activated by the MDM at lower temperatures than smaller diameter particles that have the same oxide thickness. Assuming a 3 nm shell thickness, an 80-nm-diameter Al NP would fracture at 1107 K, while a 35-nm-diameter Al NP would fracture at 1805 K based on previously published data.[43] For the particle assembly in Figure 3a, all particles reach between 937 and 1500 K (full melting) within the duration of the laser rise time of 7 μs, with a heating rate of $\sim(1-2) \times 10^8$ K/s. For the particle assembly in Figure 3b, all Al NPs that spalled reached a simulated temperature greater than 1035 K, while the Al NP that did not spall experienced incomplete melting at a temperature of 934 K. On the basis of simulation and experimental observations, the Al particle diameter, shell thickness, heating rate, and core Al temperatures of spalled Al NPs exceed the threshold values predicted by the MDM.

Additional experiments using 638- and 808-nm-wavelength laser heating were also conducted. Because of the reduced absorption cross section of Al NPs at these wavelengths (Figure 1), a laser rise time of 125 μs was used to adequately heat the NPs above their melting temperature. Both sintering and spallation events were observed when using the 638 nm wavelength; however, all experiments at 808 nm wavelength resulted in sintering or no visible change in the Al NP morphology. Thermal simulations indicate that Al NPs heat at a rate of 10^7 K/s with the 638 nm laser source and meet or exceed the melting temperature of Al. Al NPs heat at a rate of 10^6 K/s with the 808 nm laser source, but many NPs fail to reach the melting temperature of Al. Greater detail of these results and associated figures are provided in the Supporting Information. In total, the results indicate that spallation is not limited to a narrow laser wavelength spectrum but is dependent on both the heating rate and maximum temperature achieved by the Al NPs, within a regime consistent with the MDM model.

Self-propagation of the spallation reaction was also investigated. In these experiments, large clusters of Al NPs whose dimensions greatly exceeded that of the heating laser were targeted. Al NPs near the center of the cluster were directly heated, while neighboring Al NPs were heated by contact with directly radiated NPs. The AFM topology image in Figure 4a shows a large cluster of approximately 65 Al NPs centrally heated with the same laser power density and rise time as those used to trigger Al spallation previously. In this scenario, many Al NPs lie completely outside of the laser-irradiated zone or are shielded from direct line-of-sight irradiation by vertical Al NP stacking.

Evidence of two different reaction mechanisms (spallation and sintering) is displayed in Figure 4b,c, acquired after heating. The Al NPs in and above the heated region are absent after heating and are replaced by a field of smaller fragments. Small irregular fragments are observed within 2 μm from the center of the laser-heated zone, indicating spallation of the Al NPs. Note that there are no fragments beyond the field of view shown in the SEM and AFM images in Figure 4a. Sintering of many Al NPs was also evident below the heated zone after the heating event. Spherical nodes around the perimeter of the sintered mass indicate the outline of alumina shells of Al NPs that participated in the sintering.

For the loosely packed Al NP clusters examined, the spallation of Al NPs within the center of the cluster did not propagate a self-sustained chain reaction of spallation events to neighboring NPs. The lack of solid oxide particles, present in nanothermite mixtures, prevented sustained combustion. Further, initial spallation events may have propelled neighboring Al NPs away from the reaction zone. Nevertheless, we believe that Al NP spallation occurred only for the NPs located within the direct laser profile.

A histogram of the postreaction fragment heights is shown in Figure 4d. The average fragment diameter of approximately 21.9 nm is significantly smaller than the initial 120 nm Al NP diameters. The height of each small fragment in Figure 4c was converted to an equivalent hemisphere to estimate the particle mass. The large sintered particle was estimated as a sphere. With this simple estimation, a volume loss of 23% was

https://doi.org/10.1021/acsami.2c18678
ACS Appl. Mater. Interfaces 2022, 14, 55277−55284

calculated between parts a and b of Figure 4. While the measurement is only an estimate, it qualitatively suggests that large-scale mass loss from evaporation was not observed.

The spallation reaction was sufficiently energetic to induce tearing of the graphene interface layer. The tears in the graphene sheet align approximately to the same region heated by the laser but extend further than the direct irradiation zone. Small particles decorating the perimeter of the torn graphene may indicate that the graphene was consumed in a reduction reaction with the Al fuel as it escaped the alumina shell.

The reaction of large clusters similar to that shown in Figure 4a,b was also investigated using high-speed imaging. A Phantom high-speed camera was used to record the photothermal heating using a frame rate of 60606 frames/s (16.5 μs/frame). The intent of the camera was to capture potential photon emission and not to record a detailed progression of events during spallation. The synchronized system triggered the laser simultaneously with the first frame of the camera. The laser rise time of 7 μs, and the anticipated spallation reaction, was captured within the first frame. The high-speed images (Figure 4e−g) clearly show that a light-generating reaction occurred within the first exposure. The photons arose from the release of high-temperature molten Al or a combustion reaction between ejected Al and O in air. A relatively high photon intensity was required to register a response at the camera exposure time used in the experiment. The diameter of the bright spot generated by the reaction was on the order of 1 μm, similar in size to the graphene tears observed after the reaction (Figure 4c).

While AFM imaging benefited from the graphene interfacial layer, rapid Al melting and quenching on graphene promoted the formation of discrete Al NPs. Previous experiments demonstrated that surface defects in the graphene arrested the migration and aggregation of small (10 nm) molten Al droplets into larger particles.[44] Additional experiments were performed on grating substrates without the graphene interface layer to examine the potential morphological differences in the molten Al ejecta that landed on the substrate after the reaction (Figures 5 and S4). In these experiments, the exposed grating surface was a 10 nm aluminum oxide capping layer deposited by ALD to protect a Ag grating from oxidation.[44] A large cluster of approximately 50 Al NPs (Figure S4) was laser irradiated to induce spallation. SEM inspection showed that the morphology of the particle field after spallation varied significantly compared to that observed on the graphene layer. Elongated and irregularly shaped filaments were observed after the spallation reaction rather than the field of discrete particles observed when using a graphene interface. We hypothesize that the irregular geometry of the products represents molten Al jets that landed on the grating and directly quenched. Brittle aluminum oxide shells would not form such continuous, fibrous structures like those observed. Weak interaction between the alumina surface and molten Al allows the ejected material to cool relatively undisturbed on the aluminum oxide top layer of the grating.

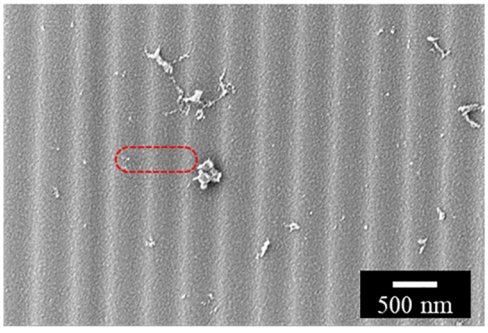

Figure 5. Representative SEM micrograph of Al NP products from a heating experiment in which graphene was not present on the optical grating substrate. The ejected material forms elongated filaments, indicating that Al was in the molten state when ejected from the host NPs. An overlaid oval represents the outline of the laser heated zone and the original location of the photothermally heated NPs.

The ejection of molten Al is consistent with the MDM, which proposes that the Al core within a NP must melt and expand prior to spallation. By extension, Al material would be molten upon ejection. The ejection of molten Al contrasts with ablation in which metal is vaporized and forms a plume that travels in the direction of the incident laser. Because the graphene sheet is the only difference between experiments, we believe that Al arrived at the substrate in the molten state regardless of the underlying substrate. If graphene was present on the landing surface, its surface energy promoted the formation of small spherical NPs before solidification. Contact with a relatively low surface energy surface, like aluminum oxide, allowed the molten Al to retain its relative shape upon solidification.

4. CONCLUSIONS

The spallation of Al NPs is demonstrated by applying localized photothermal heating to small clusters of Al NPs. Our observations show that rapid heating of isolated NPs can induce spallation in open air. The physical parameters of the NPs (120 nm diameter and 3.8 nm shell thickness), heating rate (10^7−10^8 K/s), and maximum temperature (1000−1500 K) are consistent with those required to promote the MDM. Other ultrafast excitation mechanisms, including ablation or Coulomb explosion,[45,46] require heating rates that are orders of magnitude greater than those observed here and are ruled out as possible spallation mechanisms to describe the result. The spallation reactions were not readily sustained between adjacent NPs in loose contact because large-scale sintering of NPs adjacent to the irradiated zone was observed.

We hypothesize that Al NP heating rates similar to those induced in our experiments may be achieved within the reaction of macroscale heterogeneous assemblies of Al and oxidizer NPs in nanothermite systems, thereby enabling the MDM in larger particle systems. Inducing Al NP spallation at a larger scale may further enhance the reaction rate and reaction temperature for nanothermite systems. Future parametric studies will elucidate structure−property relationships of the spallation reactions and will help to further identify and control the underlying spallation mechanisms.

■ ASSOCIATED CONTENT

Supporting Information

The Supporting Information is available free of charge at https://pubs.acs.org/doi/10.1021/acsami.2c18678.

Schematics of the experimental setup, simulated absorption cross section of Al NPs as a function of the laser wavelength and nanoparticle diameter, single-particle reaction results, 638 and 808 nm laser reaction results, additional laser information, and COMSOL simulation results (PDF)

https://doi.org/10.1021/acsami.2c18678
ACS Appl. Mater. Interfaces 2022, 14, 55277−55284

AUTHOR INFORMATION

Corresponding Authors

Matthew R. Maschmann − *Department of Mechanical and Aerospace Engineering and MU Materials Science and Engineering Institute, University of Missouri, Columbia, Missouri 65211, United States;* orcid.org/0000-0002-0740-6228; Email: MaschmannM@missouri.edu

Shubhra Gangopadhyay − *Department of Electrical Engineering and Computer Science and MU Materials Science and Engineering Institute, University of Missouri, Columbia, Missouri 65211, United States;* Email: gangopadhyays@missouri.edu

Authors

Naadaa Zakiyyan − *Department of Electrical Engineering and Computer Science, University of Missouri, Columbia, Missouri 65211, United States*

Cherian Mathai − *Department of Electrical Engineering and Computer Science, University of Missouri, Columbia, Missouri 65211, United States*

Jacob McFarland − *J. Mike Walker Department of Mechanical Engineering, Texas A&M University, College Station, Texas 77843, United States*

Complete contact information is available at: https://pubs.acs.org/10.1021/acsami.2c18678

Author Contributions

All authors contributed to the writing of the paper and data analysis. N.Z. conducted experiments. All authors have given approval to the final version of the manuscript.

Notes

The authors declare no competing financial interest.

ACKNOWLEDGMENTS

The authors acknowledge support from ARO (Grant W911NF-15-1-0136), and M.R.M. acknowledges support from NSF CMMI Award 1651538.

REFERENCES

(1) Wang, A.; Bok, S.; Thiruvengadathan, R.; Gangopadhyay, K.; McFarland, J. A.; Maschmann, M. R.; Gangopadhyay, S. Reactive Nanoenergetic Graphene Aerogel Synthesized by One-Step Chemical Reduction. *Combust. Flame* **2018**, *196*, 400−406.

(2) Thiruvengadathan, R.; Bezmelnitsyn, A.; Apperson, S.; Staley, C.; Redner, P.; Balas, W.; Nicolich, S.; Kapoor, D.; Gangopadhyay, K.; Gangopadhyay, S. Combustion Characteristics of Novel Hybrid Nanoenergetic Formulations. *Combust. Flame* **2011**, *158* (5), 964−978.

(3) Chen, Y.; Egan, G. C.; Wan, J.; Zhu, S.; Jacob, R. J.; Zhou, W.; Dai, J.; Wang, Y.; Danner, V. A.; Yao, Y.; Fu, K.; Wang, Y.; Bao, W.; Li, T.; Zachariah, M. R.; Hu, L. Ultra-Fast Self-Assembly and Stabilization of Reactive Nanoparticles in Reduced Graphene Oxide Films. *Nat. Commun.* **2016**, *7*, 12332.

(4) Young, G.; Wang, H.; Zachariah, M. R. Application of Nano-Aluminum/Nitrocellulose Mesoparticles in Composite Solid Rocket Propellants. *Propellants, Explosives, Pyrotechnics* **2015**, *40* (3), 413−418.

(5) Bezmelnitsyn, A.; Thiruvengadathan, R.; Barizuddin, S.; Tappmeyer, D.; Apperson, S.; Gangopadhyay, K.; Gangopadhyay, S.; Redner, P.; Donadio, M.; Kapoor, D.; Nicolich, S. Modified Nanoenergetic Composites with Tunable Combustion Characteristics for Propellant Applications. *Propellants, Explosives, Pyrotechnics* **2010**, *35* (4), 384−394.

(6) Thiruvengadathan, R.; Staley, C.; Geeson, J. M.; Chung, S.; Raymond, K. E.; Gangopadhyay, K.; Gangopadhyay, S. Enhanced Combustion Characteristics of Bismuth Trioxide-Aluminum Nanocomposites Prepared through Graphene Oxide Directed Self-Assembly. *Propellants, Explosives, Pyrotechnics* **2015**, *40* (5), 729−734.

(7) Tyagi, H.; Phelan, P. E.; Prasher, R.; Peck, R.; Lee, T.; Pacheco, J. R.; Arentzen, P. Increased Hot-Plate Ignition Probability for Nanoparticle-Laden Diesel Fuel. *Nano Lett.* **2008**, *8* (5), 1410−1416.

(8) Park, K.; Lee, D.; Rai, A.; Mukherjee, D.; Zachariah, M. R. Size-Resolved Kinetic Measurements of Aluminum Nanoparticle Oxidation with Single Particle Mass Spectrometry. *J. Phys. Chem. B* **2005**, *109* (15), 7290−7299.

(9) Egan, G. C.; Lagrange, T.; Zachariah, M. R. Time-Resolved Nanosecond Imaging of Nanoscale Condensed Phase Reaction. *J. Phys. Chem. C* **2015**, *119* (5), 2792−2797.

(10) Ohkura, Y.; Rao, P. M.; Zheng, X. Flash Ignition of Al Nanoparticles: Mechanism and Applications. *Combust. Flame* **2011**, *158* (12), 2544−2548.

(11) Levitas, V. I. Mechanochemical Mechanism for Reaction of Aluminium Nano- and Micrometre-Scale Particles. *Phil. Trans. R. Soc. A* **2013**, *371*, 20120215.

(12) Levitas, V. I.; Asay, B. W.; Son, S. F.; Pantoya, M. Melt Dispersion Mechanism for Fast Reaction of Nanothermites. *Appl. Phys. Lett.* **2006**, *89* (7), 071909.

(13) Levitas, V. I.; Asay, B. W.; Son, S. F.; Pantoya, M. Mechanochemical Mechanism for Fast Reaction of Metastable Intermolecular Composites Based on Dispersion of Liquid Metal. *J. Appl. Phys.* **2007**, *101* (8), 083524.

(14) Levitas, V. I.; Asay, B. W.; Son, S. F.; Pantoya, M. Mechanochemical Mechanism for Fast Reaction of Metastable Intermolecular Composites Based on Dispersion of Liquid Metal. *J. Appl. Phys.* **2007**, *101* (8), 83524.

(15) Levitas, V. I. Mechanochemical Mechanism for Reaction of Aluminium Nano- and Micrometre-Scale Particles. *Philosophical Transactions of the Royal Society A: Mathematical, Physical and Engineering Sciences* **2013**, *371* (2003), 20120215.

(16) Levitas, V. I.; Asay, B. W.; Son, S. F.; Pantoya, M. Melt Dispersion Mechanism for Fast Reaction of Nanothermites. *Appl. Phys. Lett.* **2006**, *89* (7), 071909.

(17) Sundaram, D. S.; Puri, P.; Yang, V. A General Theory of Ignition and Combustion of Nano- and Micron-Sized Aluminum Particles. *Combust. Flame* **2016**, *169*, 94−109.

(18) Henz, B. J.; Hawa, T.; Zachariah, M. R. On the Role of Built-in Electric Fields on the Ignition of Oxide Coated Nanoaluminum: Ion Mobility versus Fickian Diffusion. *J. Appl. Phys.* **2010**, *107* (2), 024901.

(19) Puri, P.; Yang, V. Thermo-Mechanical Behavior of Nano Aluminum Particles with Oxide Layers during Melting. *J. Nanopart. Res.* **2010**, *12* (8), 2989−3002.

(20) Trunov, M. A.; Schoenitz, M.; Dreizin, E. L. Effect of Polymorphic Phase Transformations in Alumina Layer on Ignition of Aluminium Particles. *Combustion Theory and Modelling* **2006**, *10* (4), 603−623.

(21) Trunov, M. A.; Schoenitz, M.; Dreizin, E. L. Ignition of Aluminum Powders under Different Experimental Conditions. *Propellants, Explosives, Pyrotechnics* **2005**, *30* (1), 36−43.

(22) Vorozhtsov, A. B.; Lerner, M.; Rodkevich, N.; Nie, H.; Abraham, A.; Schoenitz, M.; Dreizin, E. L. Oxidation of Nano-Sized Aluminum Powders. *Thermochim. Acta* **2016**, *636*, 48−56.

(23) Levitas, V. I.; Pantoya, M. L.; Dean, S. Melt Dispersion Mechanism for Fast Reaction of Aluminum Nano- and Micron-Scale Particles: Flame Propagation and SEM Studies. *Combust. Flame* **2014**, *161* (6), 1668−1677.

(24) Levitas, V. I. Burn Time of Aluminum Nanoparticles: Strong Effect of the Heating Rate and Melt-Dispersion Mechanism. *Combust. Flame* **2009**, *156* (2), 543−546.

(25) Levitas, V. I.; Hwang, Y. S. Comment on "in Situ Imaging of Ultra-Fast Loss of Nanostructure in Nanoparticle Aggregates" [J.

Appl. Phys. 115, 084903 (2014)]. *J. Appl. Phys.* **2016**, *119* (6), 066103.
(26) Mutlu, M.; Kang, J.-H.; Raza, S.; Schoen, D.; Zheng, X.; Kik, P. G.; Brongersma, M. L. Thermoplasmonic Ignition of Metal Nanoparticles. *Nano Lett.* **2018**, *18* (3), 1699−1706.
(27) Egan, G. C.; Sullivan, K. T.; Lagrange, T.; Reed, B. W.; Zachariah, M. R. In Situ Imaging of Ultra-Fast Loss of Nanostructure in Nanoparticle Aggregates. *J. Appl. Phys.* **2014**, *115* (8), 084903.
(28) Sullivan, K. T.; Chiou, W.-A.; Fiore, R.; Zachariah, M. R. In Situ Microscopy of Rapidly Heated Nano-Al and Nano-Al/WO3 Thermites. *Appl. Phys. Lett.* **2010**, *97* (13), 133104.
(29) Wood, A. J.; Chen, B.; Pathan, S.; Bok, S.; Mathai, C. J.; Gangopadhyay, K.; Grant, S. A.; Gangopadhyay, S. Influence of Silver Grain Size, Roughness, and Profile on the Extraordinary Fluorescence Enhancement Capabilities of Grating Coupled Surface Plasmon Resonance. *RSC Adv.* **2015**, *5* (96), 78534−78544.
(30) Bhatnagar, K.; Pathak, A.; Menke, D.; Cornish, P. V.; Gangopadhyay, K.; Korampally, V.; Gangopadhyay, S. Fluorescence Enhancement from Nano-Gap Embedded Plasmonic Gratings by a Novel Fabrication Technique with HD-DVD. *Nanotechnology* **2012**, *23* (49), 495201.
(31) Darr, C. M.; Korampally, V.; Chen, B.; Gangopadhyay, K.; Gangopadhyay, S. Plasmonic-Enhanced Conjugated Polymer Fluorescence Chemosensor for Trace Nitroaromatic Vapor. *Sens Actuators B Chem.* **2014**, *202*, 1088−1096.
(32) Nayak, P. K.; Hsu, C.; Wang, S.; Sung, J. C.; Huang, J. Graphene Coated Ni Fi Lms : A Protective Coating. *Thin Solid Films* **2012**, 0−4.
(33) Chen, B.; Zheng, H.; Riehn, M.; Bok, S.; Gangopadhyay, K.; McFarland, J.; Gangopadhyay, S.; Maschmann, M. R. Enhanced Fluorescence for in Situ Temperature Mapping of Photothermally Heated Aluminum Nanoparticles Enabled by a Plasmonic Grating Substrate. *Nanotechnology* **2018**, *29* (39), 395501.
(34) Sassaroli, E.; Li, K. C. P.; O'Neill, B. E. Numerical Investigation of Heating of a Gold Nanoparticle and the Surrounding Microenvironment by Nanosecond Laser Pulses for Nanomedicine Applications. *Phys. Med. Biol.* **2009**, *54* (18), 5541−5560.
(35) Yu, H.; Zhang, P.; Lu, S.; Yang, S.; Peng, F.; Chang, W. S.; Liu, K. Synthesis and Multipole Plasmon Resonances of Spherical Aluminum Nanoparticles. *J. Phys. Chem. Lett.* **2020**, *11* (15), 5836−5843.
(36) Puri, P.; Yang, V. Effect of Particle Size on Melting of Aluminum at Nano Scales. *J. Phys. Chem. C* **2007**, *111* (32), 11776−11783.
(37) Levitas, V. I.; Pantoya, M. L.; Chauhan, G.; Rivero, I. Effect of the Alumina Shell on the Melting Temperature Depression for Aluminum Nanoparticles. *J. Phys. Chem. C* **2009**, *113* (32), 14088−14096.
(38) Chen, B.; Zheng, H.; Yoon, J.; Bok, S.; Mathai, C.; Gangopadhyay, K.; Gangopadhyay, S.; Maschmann, M. R. Fluorescence-Based Temperature Sensor for in-Situ Imaging Local Temperature of Aluminum Nanoparticles on Plasmonic Gratings. *Proceedings of IEEE Sensors* **2017**, 6−8.
(39) Chen, B.; Zheng, H.; Riehn, M.; Bok, S.; Gangopadhyay, K.; Maschmann, M.; Gangopadhyay, S. In Situ Characterization of Photothermal Nanoenergetic Combustion on a Plasmonic Microchip. *ACS Appl. Mater. Interfaces* **2018**, *10* (1), 427−436.
(40) Chen, B.; Zheng, H.; Riehn, M.; Bok, S.; Gangopadhyay, K.; McFarland, J.; Gangopadhyay, S.; Maschmann, M. R. Enhanced Fluorescence for In-Situ Temperature Mapping of Photothermally Heated Aluminum Nanoparticles Enabled by a Plasmonic Grating Substrate. *Nanotechnology* **2018**, *29* (39), 395501.
(41) Zakiyyan, N.; Darr, C. M.; Chen, B.; Mathai, C.; Gangopadhyay, K.; McFarland, J.; Gangopadhyay, S.; Maschmann, M. R. Surface Plasmon Enhanced Fluorescence Temperature Mapping of Aluminum Nanoparticle Heated by Laser. *Sensors* **2021**, *21* (5), 1585.
(42) Zhang, Y.; Zhang, D.; Wu, J.; He, Z.; Deng, X. A Thermal Model for Nanosecond Pulsed Laser Ablation of Aluminum. *AIP Adv.* **2017**, *7* (7), 075010.
(43) Levitas, V. I.; Hwang, Y. S. Comment on "In Situ Imaging of Ultra-Fast Loss of Nanostructure in Nanoparticle Aggregates" [J. Appl. Phys. 115, 084903 (2014)]. *J. Appl. Phys.* **2016**, *119* (6), 066103.
(44) Chen, Y.; Egan, G. C.; Wan, J.; Zhu, S.; Jacob, R. J.; Zhou, W.; Dai, J.; Wang, Y.; Danner, V. A.; Yao, Y.; Fu, K.; Wang, Y.; Bao, W.; Li, T.; Zachariah, M. R.; Hu, L. Ultra-Fast Self-Assembly and Stabilization of Reactive Nanoparticles in Reduced Graphene Oxide Films. *Nat. Commun.* **2016**, *7* (1), 12332.
(45) Delfour, L.; Itina, T. E. Mechanisms of Ultrashort Laser-Induced Fragmentation of Metal Nanoparticles in Liquids: Numerical Insights. *J. Phys. Chem. C* **2015**, *119* (24), 13893−13900.
(46) Fennel, T.; Meiwes-Broer, K. H.; Tiggesbäumker, J.; Reinhard, P. G.; Dinh, P. M.; Suraud, E. Laser-Driven Nonlinear Cluster Dynamics. *Rev. Mod. Phys.* **2010**, *82* (2), 1793−1842.

https://doi.org/10.1021/acsami.2c18678
ACS Appl. Mater. Interfaces 2022, 14, 55277−55284